

Correlating Photovoltaic Soiling Losses to Waveband and Single-Value Transmittance Measurements

Leonardo Micheli,¹ Eduardo F. Fernandez,² Jose A. Caballero,² Greg P. Smestad,³ Gustavo Nofuentes,² Tapas K. Mallick,⁴ and Florencia Almonacid²

¹ National Renewable Energy Laboratory, Golden (CO), USA

² University of Jaén, Jaén, Spain

³ Sol Ideas Technology Development, San José (CA), USA

⁴ University of Exeter, Penryn, UK

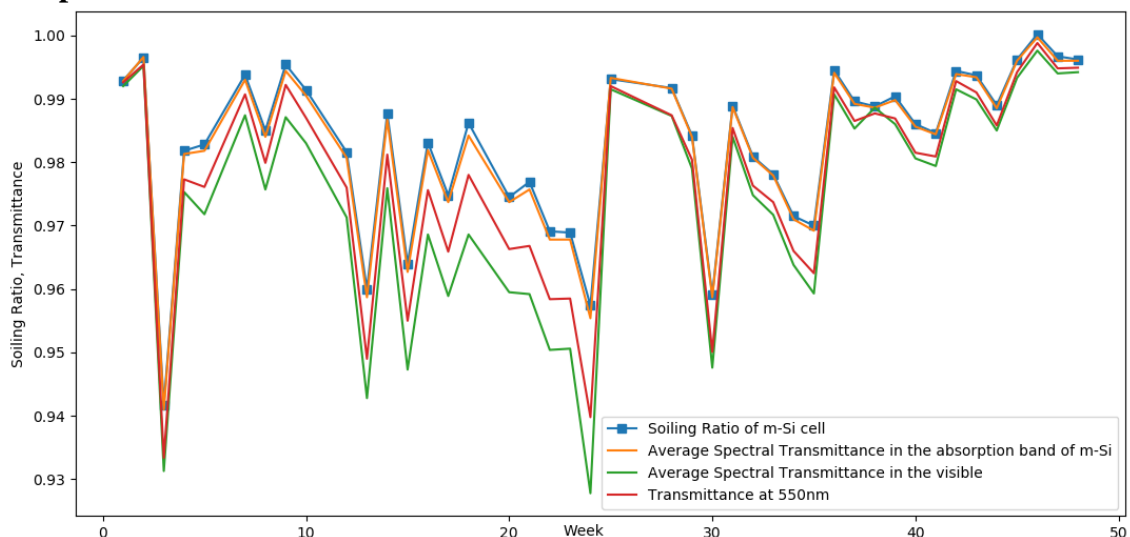
Abstract:

This paper presents the results of an investigation on the spectral losses of photovoltaic (PV) soiling. The transmittance of a glass coupon exposed to natural outdoor soiling in Jaén, southern Spain, has been measured weekly and used to estimate the soiling losses that various types of photovoltaic materials would experience if installed in the same location. The results suggest that measuring the hemispherical transmittance of the soiling accumulated on a PV glass coupon can give enough information to quantify the impact of soiling on the energy production. Each PV technology is found to have a preferred spectral region or a specific single wavelength whose transmittance could be used for the best estimation of soiling losses. Overall, considering the average spectral transmittance between the extreme wavelengths of the material-specific absorption band or the transmittance of soiling at a single wavelength between 500 and 600 nm yields the best estimations for different PV materials. The results of this work can lead to innovative approaches to detect soiling in the field and to estimate the impact of spectral changes induced by soiling on the PV energy production.

Keywords:

Soiling, Photovoltaic Reliability, Spectral Losses, Optical Transmittance

Graphical Abstract



1. Introduction

The accumulation of dust, particles, and dirt on the surface of photovoltaic (PV) modules reduces the intensity of the light transmitted through the cover glass—and, therefore, the amount of energy generated by the solar cells. This issue, known as *soiling*,

affects PV systems worldwide, causing power losses as high as 70% in the worst scenarios [1]. These losses are due to the drop in optical transmittance, because soiling absorbs part of the incoming sunlight and increases the fraction of reflected light. Moreover, soiling changes the spectrum of the transmitted light, causing larger transmittance drops in the blue region, meaning that PV technologies with different bandgaps can be differently affected by soiling [2–4].

A number of studies have investigated the causes of soiling and their correlations with environmental parameters [5–9]. These studies are important for predicting soiling losses and can lead to the identification of high and low soiling regions [10]; however, they have not taken into account the spectral effects of soiling on various PV technologies. On the other hand, most of the research to address the spectral impact of soiling has been conducted by analysing artificial soiling [2,11,12]. These studies have been crucial to understanding the effects of soiling on the performance of PV systems. But even if artificial soiling makes it possible to conduct the investigation in a controlled environment, it limits the understanding of the spectral nature of soiling in actual outdoor conditions, where types of soiling and deposition rates are different and can vary with time. The first results were recently presented [3] of a two-month experimental campaign where natural soiling was collected on glass coupons exposed in eight locations worldwide. The results of this preliminary work confirmed the higher attenuation of soiling at lower wavelengths, as previously indicated by another study based on artificial soiling [2]. In a similar study, glass coupons were exposed for one year in five different locations to understand the effectiveness of anti-soiling coatings and to quantify the abrasion due to external agents and various cleaning methods [13,14]. Despite all these important efforts, the relation between the spectral nature of soiling and its impact on each PV technology needs to be further investigated because their different absorption bands can lead to dissimilar losses among the various PV materials.

The performance of PV systems have shown a noteworthy dependence on the spectral content of the sunlight, as well as on the specific spectral absorption band of the technology [15]. Hence, measuring and analysing soiling should not disregard the spectral effects that soiling can have on various PV technologies; but determining the spectral component of soiling on fielded PV modules is still challenging. Soiling is currently quantified by using soiling stations, where the electrical output of a soiled PV device (*soiled device*) is compared with the output of the PV device for clean conditions (*control device*). Generally, two PV cells or modules are employed: one of them is regularly cleaned (*control device*), whereas the second is left to soil naturally (*soiled device*) [16]. In other geometries, only one PV cell is used as both the soiled and the control device [17]. A cover glass is placed on top of the cell to collect soiling and is removed only to take the control device measurement. Soiling stations are a simple and effective solution to measure soiling because they can directly quantify the impact of soiling on the energy output of PV modules. Unless multiple soiled devices are employed, however, soiling stations can calculate losses occurring for only a single PV technology.

Different and more affordable solutions are required to estimate the impact of soiling on the various PV technologies. Therefore, it is essential to investigate the correlations connected to the spectral nature of natural soiling, the irradiance spectra, and the soiling losses through extended experimental campaigns.

In light of the above discussion, the scope of this work is to analyse the spectral components of the soiling losses, investigating the impact of soiling on the various wavelengths of the irradiance spectrum and on the various PV technologies. This study shows how transmittance measurements can be used to estimate the soiling losses of PV

modules and aims to contribute to identifying innovative solutions and metrics to measure the soiling ratio of any PV technology.

2. Materials and Methods

2.1. Soiling spectral indices

The most commonly used metric to quantify the impact of soiling is the Soiling Ratio (r_s), which expresses the ratio between the output of a soiled PV device and the output of the same device under clean conditions [18]. The short-circuit current can be used as the electrical output if soiling is uniform, whereas the maximum power point is required for a better estimate of nonuniform soiling [5,16]. In this work, the nonuniform effects of soiling are not considered: therefore, the instantaneous soiling ratio at any time t is calculated as follows:

$$r_s(t) = \frac{I_{sc_{soil}}(t)}{I_{sc_{ref}}(t)} \quad (1)$$

where $I_{sc_{soil}}$ and $I_{sc_{ref}}$ are the short-circuit currents of a soiled PV device and of the control device, respectively. Considering this, the soiling ratio for a specific period of time T can be obtained as the average of the measured instantaneous soiling ratios by the following expression:

$$\bar{r}_s(T) = \frac{1}{n} \sum_{i=1}^n r_s(t) \quad (2)$$

where n is the number of measurements over the period of time T .

The time-dependent short-circuit currents of Equation (1), $I_{sc_{soil}}$ and $I_{sc_{ref}}$, could be obtained either experimentally from two monitored PV devices, or calculated by solving the following expressions [19]:

$$I_{sc_{ref}}(t) = A_{PV} \int_{\lambda_1}^{\lambda_2} E_G(\lambda, t) SR(\lambda) d\lambda \quad (3)$$

$$I_{sc_{soil}}(t) = A_{PV} \int_{\lambda_1}^{\lambda_2} E_G(\lambda, t) \tau_{soiling}(\lambda, t) SR(\lambda) d\lambda \quad (4)$$

where λ_1 and λ_2 are the lower and upper limits of the absorption band of each PV device's absorber material (i.e., m-Si, CdTe, CIGS), A_{PV} is its active area, $SR(\lambda)$ is the spectral response, $\tau_{soil}(\lambda, t)$ is the hemispherical spectral transmittance of soiling accumulated on the surface of the soiled device, and $E_G(\lambda, t)$ is the actual spectral distribution of the solar irradiance on the plane of the PV panels.

At the same time, the average spectral transmittance (AST) of soiling across a specific spectral waveband can be calculated with the following relationship:

$$AST_i(t) = \frac{1}{\lambda_{2i} - \lambda_{1i}} \int_{\lambda_{1i}}^{\lambda_{2i}} \tau_{soiling}(\lambda, t) d\lambda \quad (5)$$

where λ_{1i} and λ_{2i} , respectively, are the shortest and longest wavelengths in the selected waveband i . The various wavebands considered in this work describe either a specific spectral region or an individual PV material's absorption band and are listed in Table 1. Note that the lower and upper limits of the spectral region bands are defined by considering the absorption bands of the PV materials; the shortest and longest wavelengths selected are, respectively, 300 nm for the ultraviolet and 1,240 nm for the near-infrared regions.

Table 1. Wavebands considered in the present study.

Waveband		λ_1 [nm]	λ_2 [nm]
Spectral regions	Ultraviolet (UV)	300	400
	Visible (VIS)	400	700
	Near-infrared (NIR)	700	1,240
PV material absorption bands	Monocrystalline silicon (m-Si)	340	1,190
	Polycrystalline silicon (p-Si)	310	1,180
	Amorphous silicon (a-Si)	300	790
	Cadmium telluride (CdTe)	310	880
	Copper indium gallium diselenide (CIGS)	370	1,240
	Perovskite	300	820

2.2. Experimental campaign

2.2.1 Location

A 48-week experiment—from January 2017 to January 2018—was conducted on the roof of the A3-building at the University of Jaén, in Jaén, Spain (latitude 37°49’N, longitude 3°48’W, elev. 457 m). Jaén is a medium-size town located in southern Spain with a high annual energy resource (more than 1,800 kWh/m²), and extreme temperatures ranging from less than 5°C in winter to more than 40°C in summer [20]. Atmospheric conditions are described by low-medium values of precipitable water, turbidity, and airborne particulate matter, even if this can periodically reach unusually high values due to specific and stochastic events such as Saharan dust storms or the burning of branches from olive groves in the local region [21].

2.2.2 Transmittance

One Diamant® low-iron glass coupon 4 cm × 4 cm in size and 3 mm thick from Saint-Gobain Glass was placed horizontally outdoors to capture natural dust (*Soiled Coupon*). The coupon was never cleaned, and its hemispherical transmittance was measured weekly within a wavelength range between 300 and 1,240 nm, using a Lambda 950 spectrophotometer with a 60-mm-diameter integrating sphere at the Center of Scientific-Technical Instrumentation (CICT) of the University of Jaén. The general arrangement is outlined in Figure 1. Another sample (*Control Coupon*) was stored in a dust-free box to prevent its optical transmittance characteristics from being adversely affected from accidental soiling, and it was used as the baseline for each measurement. Its transmittance also allowed us to check the quality and repeatability of weekly measurements. The soiling transmittance is obtained from the measurement as follows:

$$\tau_{soiling}(\lambda) = \frac{\tau_{soil}(\lambda)}{\tau_{ref}(\lambda)} \quad (6)$$

where $\tau_{soil}(\lambda)$ and $\tau_{ref}(\lambda)$ are the spectral transmittance of the Soiled Coupon and Control Coupon, respectively, at the wavelength range described above.

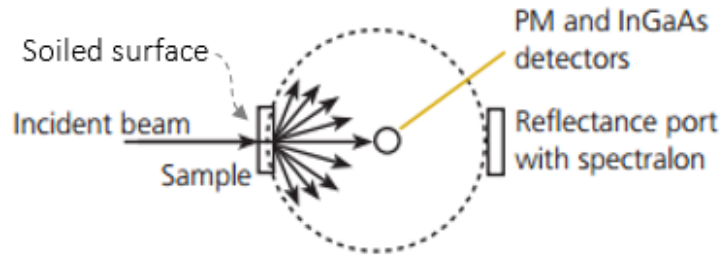


Figure 1. Schematic of the hemispherical transmittance measurement using the integrating sphere.

2.2.3 Irradiance

The global spectral irradiance between the 350-nm and 1,050-nm wavelength band was also measured at 5-minute intervals using a weatherproof spectroradiometer (EKO@MS700) oriented south and tilted 30° above the horizontal. This angle has been selected to maximize the collected irradiation over the year [22]. This instrument presents a spectral resolution of 10 nm and a temperature dependency within $\pm 1\%$ for temperatures ranging from -20°C to $+50^{\circ}\text{C}$. The expanded uncertainties of the instrument are $\pm 10.90\%$, $\pm 4.20\%$, and $\pm 4.10\%$, respectively, for the 350–450-nm, 450–900-nm, and 900–1,050-nm wavebands, according to the certificate of calibration provided by the manufacturer. We mention that the absorption bands of some PV devices (see Table 1 and Figure 2) go beyond the measurement range of the spectroradiometer. This limitation has been overcome by using the methodology proposed by Martín and Ruiz [23]. The missing wavebands have been estimated by scaling the AM1.5G reference spectrum according to the ratio between the integrated actual and referenced spectral irradiance in the range of 700–1,050 nm. This methodology was used and validated by Nofuentes *et al.* [24] to elucidate the impact of the spectral mismatch factor (MM) on the average photon energy (APE). In addition, all measurements recorded at irradiance levels below 300 W/m^2 have not been taken into account so as to avoid the non-linear performance of PV cells as such low irradiance values [24–26]. Nevertheless, these low irradiance levels do not play a significant role in the annual electrical output of PV systems at locations with a high-energy solar resource, such as the location considered in this study [27–29]. In addition, all the measurements with an incident angle equal to or greater than 60° have been removed to reduce the impact of the increased glass Fresnel reflection [30]. This approach also automatically excludes conditions in which the impact of soiling has been found to be strongly related to the angle of incidence [31].

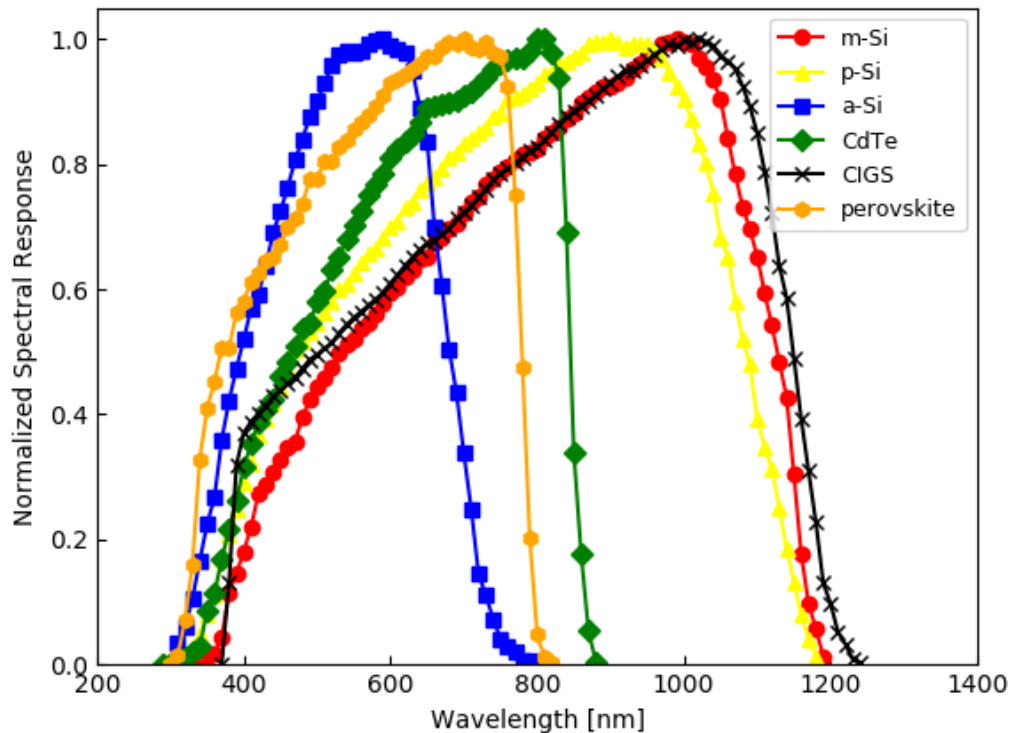


Figure 2. Normalized spectral response of the six PV materials considered in this study (m-Si: mono-crystalline silicon; p-Si: poly-crystalline silicon; a-Si: amorphous silicon; CdTe: cadmium telluride; CIGS: copper indium gallium diselenide; perovskite) [21,33].

2.3. Methodology

PV materials have different spectral absorption bands and different spectral responses, as shown in Figure 2, for the six PV technologies investigated in this study. In addition, the transmittance of soiling has a nonuniform spectral distribution, with higher losses at shorter wavelengths, as shown also in Figure 3. This means that soiling can have different impact on the various PV materials, which is a result of the product of the spectral response with the time-dependent irradiance and soiling transmittance spectra. Note that discussing the effects of soiling on the different PV technologies is outside the scope of this paper, which only focuses on the relationship between soiling losses and soiling transmittance. With this in mind, we have established the following procedure to conduct the analysis presented in this paper:

1. Measuring the spectral transmittance of soiling ($\tau_{\text{soiling}}(\lambda)$) collected on the Soiled Coupon once per week by using Equation (6).
2. Calculating the soiling ratios by using Equations (1), (2), (3), and (4). The SR of each PV device, the $\tau_{\text{soiling}}(\lambda)$ obtained in step 1, and the irradiance spectra recorded during the same day are used as inputs.
3. Estimating the average transmittance of soiling (AST(λ)) for the regions of the spectrum and the PV devices listed in Table 1 using Equation (5) and $\tau_{\text{soiling}}(\lambda)$.
4. Comparing the soiling ratios obtained in step 2 for the different wavebands investigated in step 3 by using several standard statistical metrics.

This paper considers only the hemispherical transmittance of soiling. Even if less affected by soiling than the direct component [3], the hemispherical transmittance has been preferred because it is more representative of the actual effect of soiling on power conversion. Photovoltaic modules, indeed, can convert both the direct and diffuse components of the light, as well as the part that is scattered by soiling. The hemispherical

transmittance measurement can capture all these components. Therefore, any transmittance mentioned in the document must be considered as hemispherical.

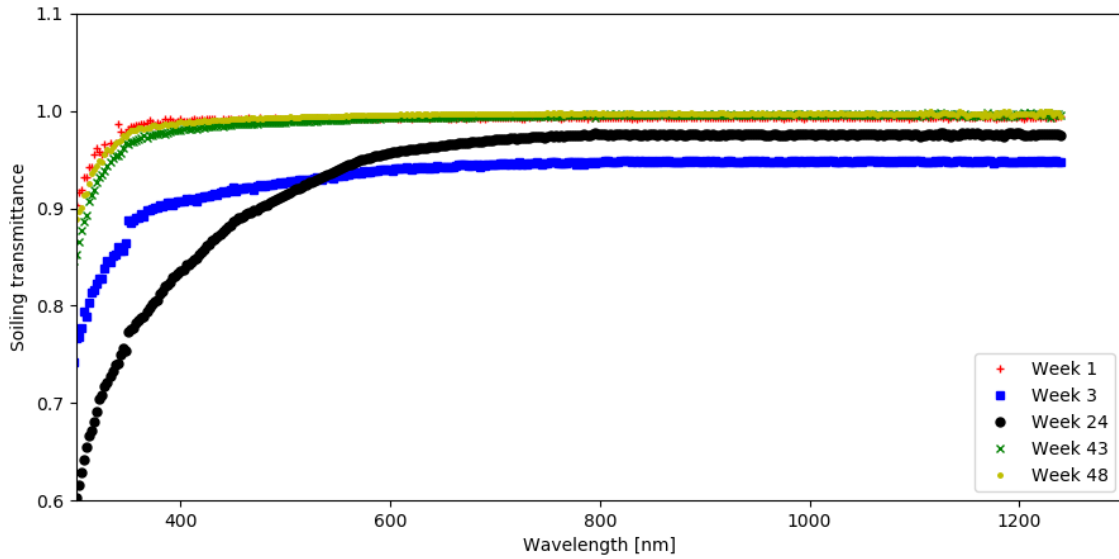


Figure 3. Soiling transmittance, calculated by using Equation (6), for five representative weeks of the data collection period.

3. Results and Discussion

In this section, two different analyses are carried out. First, the soiling ratio is estimated for three different spectral regions and for a region specific to the spectral response band of each PV material. Second, an estimation is made by using a single wavelength to facilitate the quantification of the spectral impact of soiling as accurately as possible with a simple measurement. Each analysis is conducted by using different statistical indexes: the determination coefficient (R^2), the mean absolute percentage error (MAPE), and the mean percentage error (MPE). These magnitudes have been calculated by means of the following expressions [32]:

$$R^2 = \left(\frac{\sum_{i=1}^n (r_s - \bar{r}_s)(Z - \bar{Z})}{\sqrt{\sum_{i=1}^n (r_s - \bar{r}_s)^2 \sum_{i=1}^n (Z - \bar{Z})^2}} \right)^2 \quad (7)$$

$$MAPE (\%) = \frac{100}{n} \sum_{i=1}^n \left| \frac{Z - r_s}{r_s} \right| \quad (8)$$

$$MPE (\%) = \frac{100}{n} \sum_{i=1}^n \frac{Z - r_s}{r_s} \quad (9)$$

where n is the number of soiling ratio data points and Z represents the soiling ratio predicted through the average spectral transmittance or a single wavelength transmittance data points used to estimate the soiling ratio. The coefficient of determination measures the quality of the fit between the soiling ratios and the Z values. It has a value of 1 if the Z points predict the soiling ratios with a linear equation with no error, and it has a value of 0 if no linear correlation exists between the soiling ratios and the Z points. The MAPE measures the average value of the absolute errors between the soiling ratios and their calculated values (Z points). It has a value of 0 if the soiling ratios and the Z value are the same, and it increases depending on the number and the magnitude of the errors in the prediction. The MPE is a metric calculated similarly to MAPE, but it takes into account the actual values of the errors instead of their absolute values, and it gives information on

any systematic bias in the prediction: it is positive if the predicted values tend to overestimate soiling; otherwise, it is negative.

3.1. Analysis of spectral waveband

In this subsection, we investigate the correlations between the average spectral transmittance across different spectral bands and the soiling ratio. In Figure 4, the soiling ratio, calculated weekly using Eq. (2), is plotted against the average spectral transmittance of the ultraviolet, visible, and near-infrared regions, as given by Eq. (5). The best linear fits and the coefficients of determination (R^2) obtained for each PV technology in each region are also reported in the charts. For better readability, only three PV materials with high (a-Si), intermediate (CdTe) and low (m-Si) energy gaps are represented. Figure 5 shows the current density of the three materials exposed to the reference AM1.5 global irradiance. The data for all technologies, inclusive of MAPE and MPE values, are reported in Table 2.

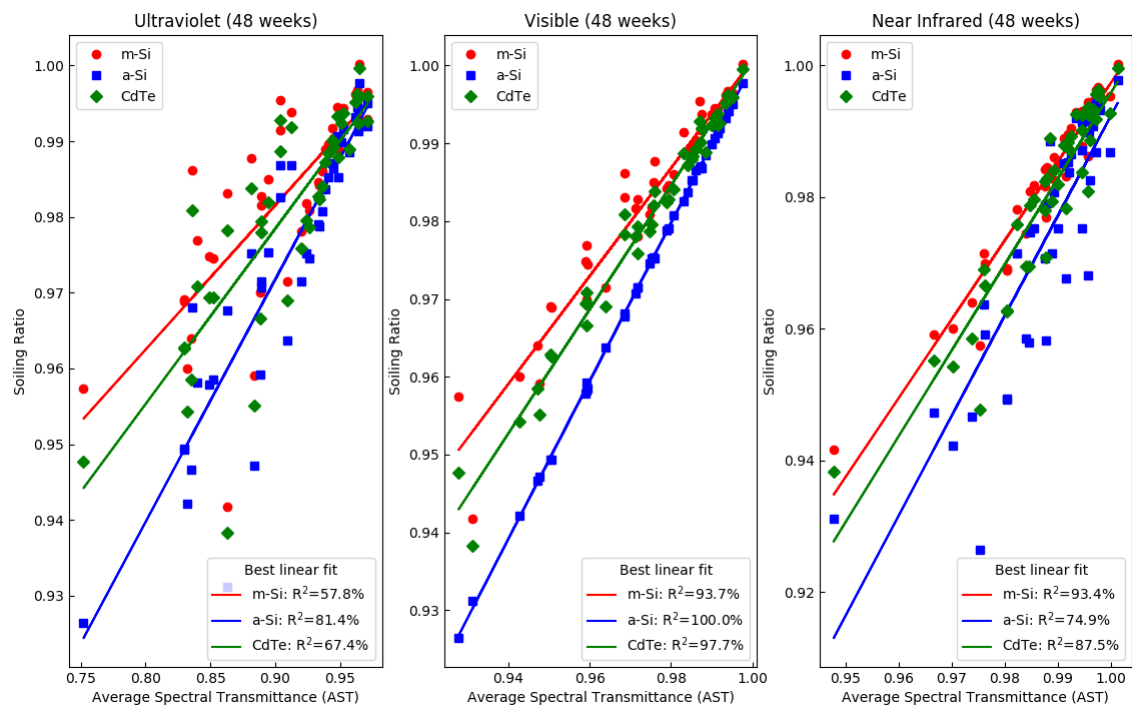


Figure 4. Soiling ratio vs average spectral transmittance in the ultraviolet (left), visible (centre), and near-infrared (right) spectral regions for three representative PV materials.

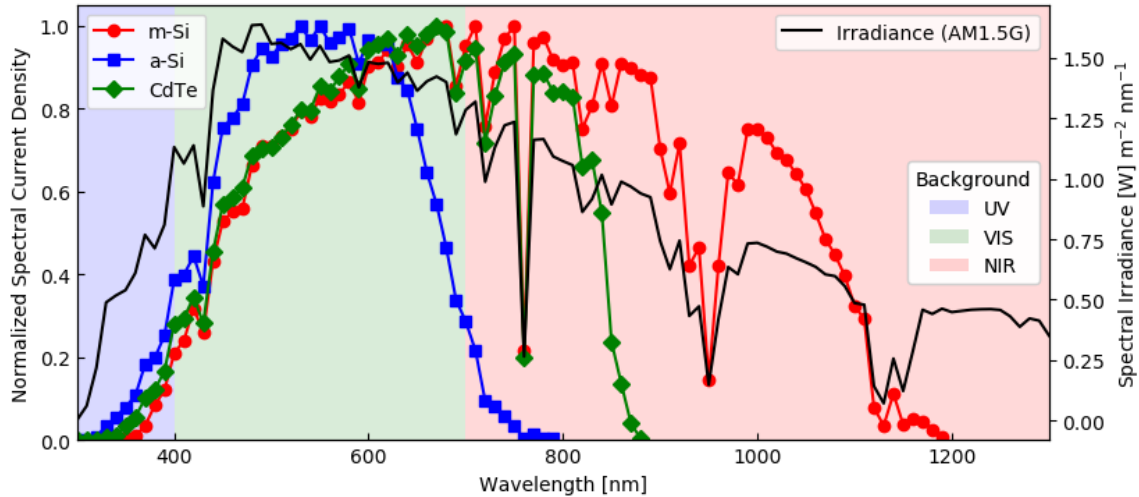


Figure 5. Current density of three PV materials under the standard AM1.5 global irradiance (ASTM G173 – 03) on the left y-axis. The current density is obtained as product of the irradiance and the spectral response of each material. The irradiance spectrum (black line) is plotted on the right y-axis. The colors in the background mark the three spectral regions: ultraviolet (UV), visible (VIS), and near-infrared (NIR).

Table 2. Coefficient of determination (R^2), mean absolute percentage error (MAPE), and mean percentage error (MPE) between soiling ratio and transmittance in three spectral regions for the six PV materials considered.

Material	Ultraviolet (300–400 nm)			Visible (400–700 nm)			Near-Infrared (700–1,240 nm)		
	R^2 (%)	MAPE (%)	MPE (%)	R^2 (%)	MAPE (%)	MPE (%)	R^2 (%)	MAPE (%)	MPE (%)
m-Si	57.8	7.76	-7.76	93.7	0.88	-0.88	93.4	0.52	0.52
p-Si	61.3	7.69	-7.69	95.4	0.80	-0.80	91.5	0.60	0.60
a-Si	81.4	6.94	-6.94	100	0.04	0.03	74.9	1.45	1.45
CdTe	67.4	7.50	-7.50	97.7	0.59	-0.59	87.5	0.81	0.81
CIGS	60.7	7.71	-7.71	95.1	0.82	-0.82	91.9	0.58	0.58
perovskite	77.6	7.15	-7.15	99.8	0.20	-0.20	79.0	1.21	1.21

As shown, the quality of the best fit varies with both the spectral region and the PV technology. Using the UV portion of the light lowers the correlation for all the technologies, with MAPE percentages of 7% or higher. In particular, the MPE values are all found to be negative, meaning that AST returns lower values than the actual soiling ratios. This is not surprising because the UV region contributes little to the current generation in PV modules because it represents only a limited portion of the solar irradiance spectrum. Moreover, all the PV technologies have low spectral response in this region (Figure 5), whereas soiling causes dramatic transmittance drops [2,3]. The best result for the UV is found for a-Si because this is the technology with the highest absorption at the lowest wavelengths (Figure 5).

Overall, the best results are obtained if the visible AST is considered, with the maximum R^2 achieved by a-Si, perovskite, and CdTe technologies; most of their absorption occurs in this region (Figure 5). All the technologies have low MAPE (<1%), with a-Si reaching values lower than 0.1%. Soiling losses of a-Si technologies can be predicted with high accuracy by measuring the visible AST only.

The low-energy bandgap materials (m-Si, p-Si, CIGS) are the only technologies to have R^2 above 90% in both the visible and near-infrared regions. This is because the solar

irradiance is high and their spectral response is significant both in the visible and at higher wavelengths (Figure 5). Their MAPE is lower in the NIR than in the visible. On the other hand, R^2 drops and the MAPE increases for a-Si in the NIR because of the very limited spectral response in this region.

The visible portion of the spectrum returns the best results if materials from various energy bandgaps are investigated, even if it introduces a significant negative offset (MAPE $\geq 0.8\%$) for low-energy gap materials. The results for some PV technologies can be enhanced by using the specific material absorption band instead of a spectral region for calculating AST (Figure 6). Indeed, R^2 of at least 98%, MAPE between 0.04% and 0.65%, and negative MPE up to -0.65% for all the materials (with the worst values for a-Si and perovskite) are the result by using the PV absorption bands in calculating AST. The negative bias is because the spectral response of each material slowly grows with the wavelength from UV to visible and/or the NIR, until it peaks and dramatically drops after that (Figure 5). PV technologies have limited spectral response in that wide pre-peak region, and the irradiance region has the lowest intensity in UV. On the other hand, the AST is calculated as a simple average of the waveband transmittance (see Equation 8), giving the same weight to all the wavelengths in the spectral range, independently of the spectral response and irradiance. So, the soiling-intensive short-wavelength band has a larger impact on the AST than on the actual PV modules, leading to an overestimation of the soiling (represented by lower predicted, Z , than actual soiling ratios, r_s).

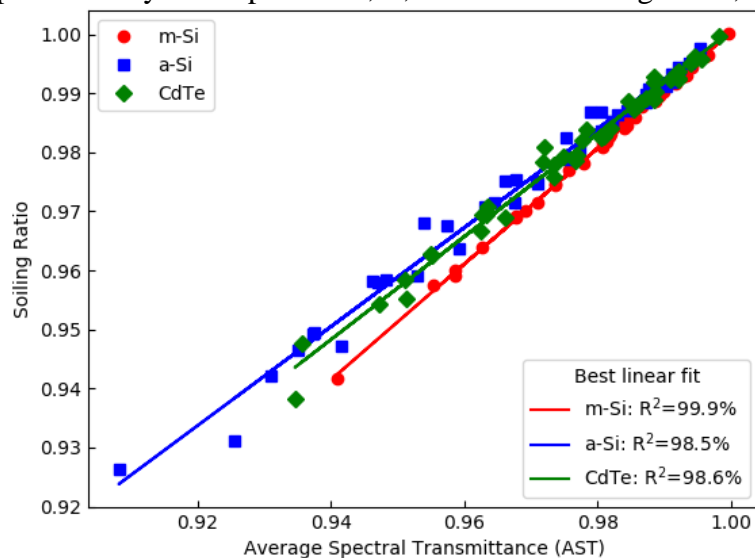


Figure 6. Soiling ratio vs Average spectral transmittance for three representative PV material absorption bands.

3.2. Analysis of the transmittance at single wavelength

In the previous subsection, we showed how we use the average transmittance of a waveband to estimate the soiling losses occurring over the whole irradiance spectrum for different PV technologies. In this section, we investigate if the transmittance of a single wavelength can be used for the same purpose. For this reason, the same analysis presented earlier has been repeated using wavelengths at 50-nm steps between 300 nm and 1,000 nm. All the results are plotted in Figure 7. As can be seen, the maximum R^2 ($\geq 99\%$) and minimum MAPE are obtained if the hemispherical transmittance at single wavelengths between 500 and 650 nm is used to estimate the soiling losses of PV materials.

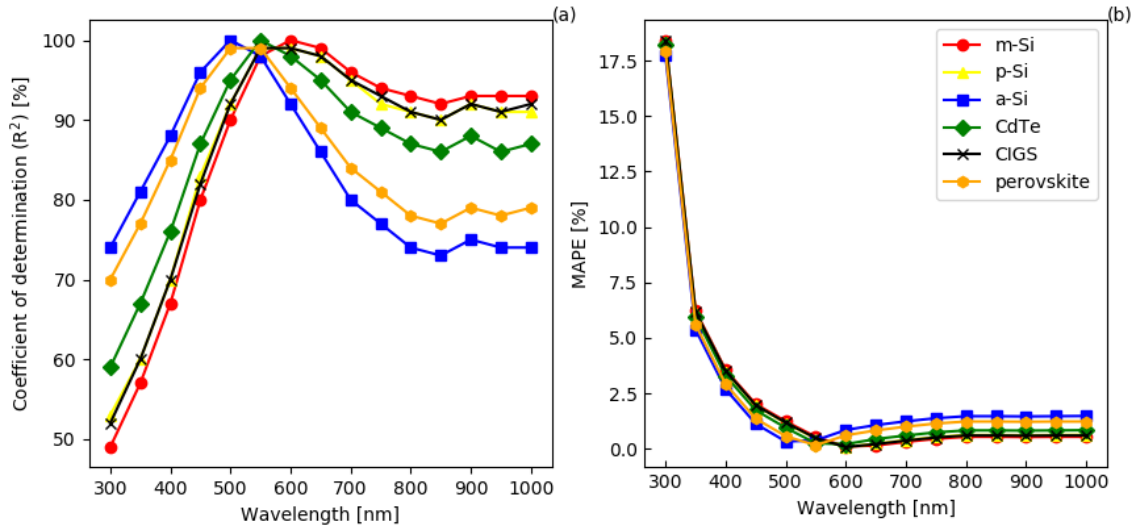


Figure 7. (a) Coefficients of determination and (b) MAPE obtained when soiling losses for various PV technologies are estimated using a single hemispherical transmittance wavelength.

The best-performing wavelengths for each material are reported in Table 3. Except for CdTe, the wavelengths that maximize the R^2 for a material are those that minimize the MAPE, as well. (CdTe’s MAPE = 0.21% and $R^2 = 98.3\%$ at 600 nm.) The results show that $R^2 \geq 99\%$ and MAPE < 0.35% can be achieved for any PV technology if the transmittance of soiling at a specific wavelength is considered. This suggests that the soiling losses for each material could be ideally predicted by using a single-wavelength measurement with high accuracy. Table 3 suggests that the most appropriate wavelength of each technology can be selected by considering their energy bands: 500 nm for high (a-Si), 550 nm to 600 nm for intermediate (CdTe and perovskite), and 600 nm for low (m-Si, p-Si, and CIGS) energy bandgaps. All materials, except a-Si, show lower MAPE if the transmittance of a single wavelength is used instead of the AST of any of the wavebands investigated in the previous section.

Table 3. Single wavelengths that maximize the coefficient of determination for each PV technology.

Material	Maximum R^2		
	Wavelength [nm]	R^2 (%)	MAPE (%)
m-Si	600	99.7	0.10
p-Si	600	99.4	0.08
a-Si	500	99.7	0.33
CdTe	550	99.8	0.25
CIGS	600	99.5	0.08
perovskite	550	99.0	0.16

If soiling needs to be determined for more than one PV technology with the same measurement, then it is of interest to find a single wavelength that minimizes the overall error. The coefficients of determination, MAPE, and MPE for each PV technology at the most significant wavelengths found earlier (500, 550, and 600 nm) are reported in Table 4. The transmittance measured at any of the selected wavelengths achieves $R^2 \geq 90\%$ when compared to the soiling ratio of any material. Despite that, the average R^2 is lower at the extremes of the selected range. 500 nm favours a-Si and perovskite, but it yields worse predictions for other technology; in contrast, 600 nm maximizes low-energy-band materials, but negatively affects a-Si and perovskite. Moreover, 500 nm shows negative

MPE for all the technologies (transmittance systematically lower than soiling ratio) and, in some cases, MAPE is higher than 1%. Therefore, 500 nm seems to be beneficial only if a-Si is investigated. On the other hand, 600 nm should be considered if low-energy bandgap materials are under investigation. Acceptable results are yielded at 600 nm for CdTe, even if 550 nm maximizes its results. Overall, 550 nm can be considered the most convenient if soiling losses need to be determined from one simple wavelength because R^2 is equal to or higher than 98% for all the materials.

Table 4. Coefficient of determination (R^2), mean absolute percentage error (MAPE), and mean percentage error (MPE) between soiling ratio and transmittance in three spectral regions for the five PV materials considered.

Material	500 nm			550 nm			600 nm		
	R^2 (%)	MAPE (%)	MPE (%)	R^2 (%)	MAPE (%)	MPE (%)	R^2 (%)	MAPE (%)	MPE (%)
m-Si	90.3	1.24	-1.24	98.3	0.54	-0.54	99.7	0.10	-0.08
p-Si	92.3	1.16	-1.16	99.1	0.46	-0.46	99.4	0.08	0.00
a-Si	99.7	0.33	-0.33	97.9	0.38	0.38	91.6	0.85	0.85
CdTe	95.4	0.95	-0.95	99.8	0.25	-0.25	98.3	0.21	0.21
CIGS	92.0	1.18	-1.18	99.0	0.48	-0.48	99.5	0.08	-0.02
perovskite	98.9	0.57	-0.57	99.0	0.16	0.14	94.0	0.61	0.61

The results of this work suggest that soiling detection could be performed by using average waveband or single-wavelength transmittance measurements. The time series of the soiling ratio and of the various indexes here analyzed are shown in Figure 8 for three representative PV materials. Each material has a waveband or wavelength that maximizes the soiling loss prediction, as summarized in Table 5. This can lead to the development of innovative soiling detecting systems, based on transmittance measurements, that might be able to quantify the impact of soiling on different PV technologies.

Table 5. Summary of the best correlations obtained for each material between the soiling ratios and the various parameters investigated.

Material	Best results
m-Si	Transmittance at 600 nm or AST at specific absorption band
p-Si	Transmittance at 600 nm
a-Si	AST in the visible
CdTe	Transmittance at 550 or 600 nm
CIGS	AST at specific absorption band, followed by transmittance at 600 nm
perovskite	Transmittance at 550 nm, followed by AST in the visible

4. Conclusions

One glass coupon was exposed outdoors for 48 weeks in Jaén, a city in southern Spain. The spectral transmittance of the soiling accumulated on the coupon was measured weekly to evaluate the transmittance drop due to soiling and to estimate the losses that this would have caused on PV modules. We investigated the ability to predict soiling losses of different PV materials using only transmittance data. The results show that soiling at a location can, in principle, be estimated by using the transmittance at selected wavelength ranges—or, even at a single wavelength—with high accuracy.

In most cases, the best estimations are obtained if the transmittance is measured at a wavelength within 500 and 600 nm. Each energy-band category shows a range in which

the results are optimized: 500 nm for high (a-Si), 550 nm to 600 nm for intermediate (CdTe and perovskite), and 600 nm for low (m-Si, p-Si and CIGS) energy bandgaps. Alternatively, the average spectral transmittance over the specific material absorption band returns the best soiling estimates compared to the average transmittance of the spectral regions for all materials, except for amorphous silicon and perovskite cells. Among the three regions of the solar irradiance, the best results are obtained for the visible band ($R^2 \geq 94\%$ for all the materials), even if this introduces a systematic offset in calculating the soiling ratio for low-energy-bandgap materials (see m-Si time series in Figure 8).

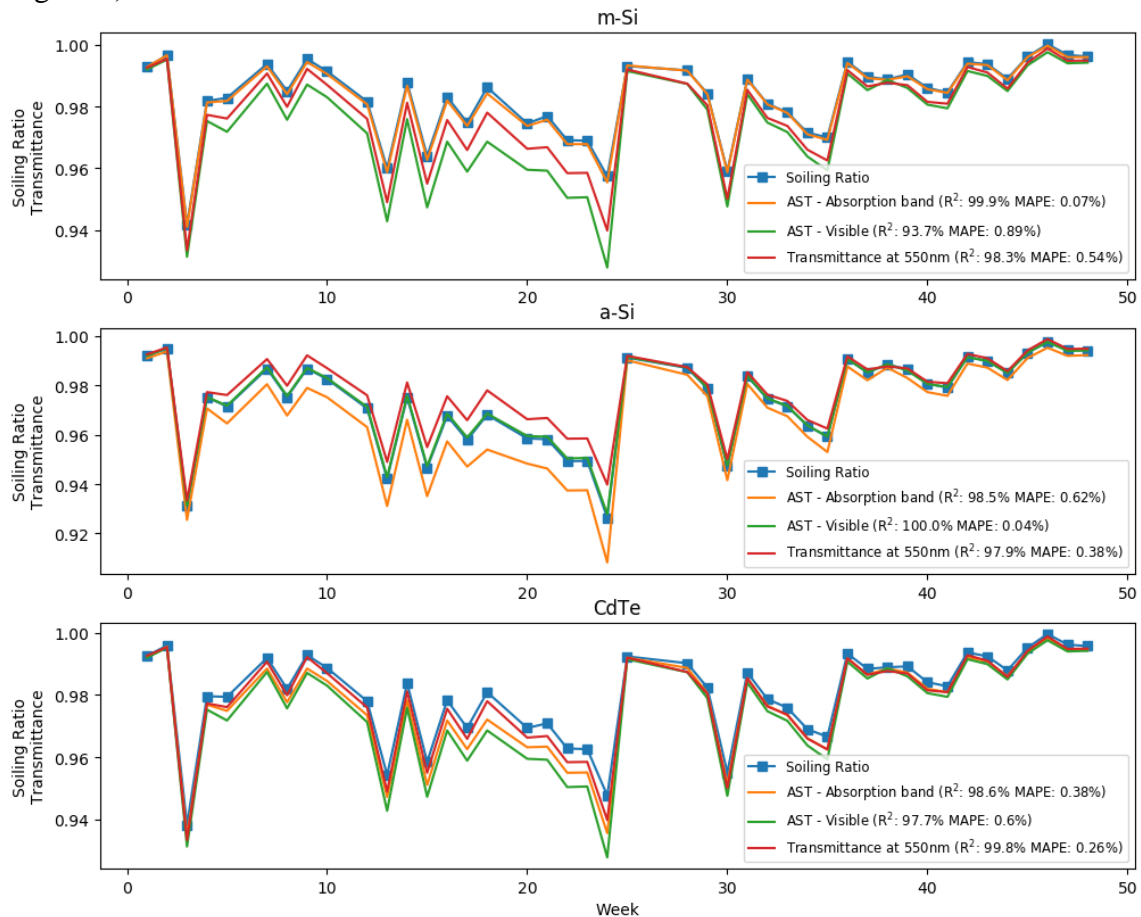


Figure 8. Weekly time series of soiling ratio, average spectral transmittances (AST) over the specific material absorption band, and over the visible spectrum and single-wavelength transmittance at 550 nm for monocrystalline silicon (m-si, high-energy material), cadmium telluride (CdTe, intermediate-energy material), and amorphous silicon (a-Si, low-energy material).

This work suggests that the impact of soiling on the electrical output of PV cells can be estimated, with good accuracy, by using broadband or even single-wavelength optical transmittance measurements. These results can lead to the development of innovative spectral soiling-detector devices. The data collection used for this analysis took place for 48 weeks at only one location that, over a one-year period, is exposed to various types of soiling (Saharan dust, olive tree pollen and smoke, and urban particulate matter); however, similar investigations should be replicated in different locations. Moreover, the transmittance was measured at zero angle of incidence, whereas in PV modules deployed in the field, the transmittance of soiling varies daily and hourly (depending on the angle of incidence). Therefore, further studies should be conducted to consider these effects and to confirm the findings of the present study.

Acknowledgments

This work was authored in part by Alliance for Sustainable Energy, LLC, the manager and operator of the National Renewable Energy Laboratory for the U.S. Department of Energy (DOE) under Contract No. DE-AC36-08GO28308. Funding was provided in part by the U.S. Department of Energy’s Office of Energy Efficiency and Renewable Energy (EERE) under Solar Energy Technologies Office (SETO) Agreement Number 30311.

This work was conceived and partially funded as part of the “Global investigation on the spectral effects of soiling losses” project, financed under the UK EPSRC SUPERGEN SuperSolar Hub’s “International and industrial engagement fund.”

The views expressed in the article do not necessarily represent the views of the DOE or the U.S. Government. The U.S. Government retains and the publisher, by accepting the article for publication, acknowledges that the U.S. Government retains a nonexclusive, paid-up, irrevocable, worldwide license to publish or reproduce the published form of this work, or allow others to do so, for U.S. Government purposes.

This study is partially based upon work from COST Action PEARL PV (CA16235), supported by COST (European Cooperation in Science and Technology). COST (European Cooperation in Science and Technology) is a funding agency for research and innovation networks. Our Actions help connect research initiatives across Europe and enable scientists to grow their ideas by sharing them with their peers. This boosts their research, career and innovation, see www.cost.eu.

References

- [1] T. Sarver, A. Al-Qaraghuli, L.L. Kazmerski, A comprehensive review of the impact of dust on the use of solar energy: History, investigations, results, literature, and mitigation approaches, *Renew. Sustain. Energy Rev.* 22 (2013) 698–733. doi:10.1016/j.rser.2012.12.065.
- [2] H. Qasem, T.R. Betts, H. Müllejans, H. AlBusairi, R. Gottschalg, Dust-induced shading on photovoltaic modules, *Prog. Photovoltaics Res. Appl.* 22 (2014) 218–226. doi:10.1002/pip.2230.
- [3] L. Micheli, E.F. Fernández, G.P. Smestad, H. Alrashidi, N. Sarmah, I.A.I. Hassan, et al., A unified global investigation on the spectral effects of soiling losses of PV glass substrates : preliminary results, in: *IEEE 44th Photovolt. Spec. Conf.*, IEEE, Washington, D.C., 2017: pp. 3–8.
- [4] D.C. Miller, L.M. Gedvilas, B. To, C.E. Kennedy, S.R. Kurtz, Durability of Poly (Methyl Methacrylate) Lenses Used in Concentrating Photovoltaic Modules Preprint, in: *SPIE Sol. Energy + Technol.*, 2010.
- [5] L. Micheli, M. Muller, An investigation of the key parameters for predicting PV soiling losses, *Prog. Photovoltaics Res. Appl.* 25 (2017) 291–307. doi:10.1002/pip.2860.
- [6] L. Micheli, D. Ruth, M. Muller, Seasonal Trends of Soiling on Photovoltaic Systems, in: *2017 IEEE 44th Photovolt. Spec. Conf.*, IEEE, Washington, D.C., 2017.
- [7] W. Javed, B. Guo, B. Figgis, Modeling of photovoltaic soiling loss as a function of environmental variables, *Sol. Energy.* 157 (2017) 397–407. doi:10.1016/j.solener.2017.08.046.
- [8] F.A. Mejia, J. Kleissl, Soiling losses for solar photovoltaic systems in California, *Sol. Energy.* 95 (2013) 357–363. doi:10.1016/j.solener.2013.06.028.
- [9] A. Kimber, L. Mitchell, S. Nogradi, H. Wenger, The Effect of Soiling on Large Grid-Connected Photovoltaic Systems in California and the Southwest Region of the United States, in: *Photovolt. Energy Conversion, Conf. Rec. 2006 IEEE 4th*

- World Conf., 2006: pp. 2391–2395.
- [10] L. Micheli, M.G. Deceglie, M. Muller, Map and regional analysis of photovoltaic soiling across the United States, in: 7th World Conf. Photovolt. Energy Convers., IEEE, Waikoloa, HI, 2018.
- [11] P.D. Burton, B.H. King, D. Riley, Predicting the spectral effects of soils on high concentrating photovoltaic systems, *Sol. Energy*. 112 (2015) 469–474. doi:10.1016/j.solener.2014.11.022.
- [12] P.D. Burton, B.H. King, Spectral Sensitivity of Simulated Photovoltaic Module Soiling for a Variety of Synthesized Soil Types, *IEEE J. Photovoltaics*. 4 (2014) 890–898. doi:10.1109/JPHOTOV.2014.2301895.
- [13] S. Toth, M. Muller, D.C. Miller, H. Moutinho, B. To, L. Micheli, et al., Soiling and cleaning: Initial observations from 5-year photovoltaic glass coating durability study, *Sol. Energy Mater. Sol. Cells*. In Press (2018).
- [14] A. Einhorn, L. Micheli, D.C. Miller, L.J. Simpson, M. Muller, S. Toth, et al., Optical microscopy study of soiling on PV glass: Evaluation of possible mitigation strategies, in: 7th World Conf. Photovolt. Energy Convers., Waikoloa, HI, 2018.
- [15] P.M. Rodrigo, E.F. Fernández, F.M. Almonacid, P.J. Pérez-Higueras, Quantification of the spectral coupling of atmosphere and photovoltaic system performance: Indexes, methods and impact on energy harvesting, *Sol. Energy Mater. Sol. Cells*. 163 (2017) 73–90. doi:http://dx.doi.org/10.1016/j.solmat.2017.01.018.
- [16] M. Gostein, T. Duster, C. Thuman, Accurately Measuring PV Soiling Losses With Soiling Station Employing Module Power Measurements, in: IEEE 42nd Photovolt. Spec. Conf., 2015.
- [17] T. Curtis, S. Tatapudi, G. Tamizhmani, Design and Operation of a Waterless PV Soiling Monitoring Station, in: 7th World Conf. Photovolt. Energy Convers., IEEE, Waikoloa, HI, 2018.
- [18] International Electrotechnical Commission, Photovoltaic system performance – Part 1: Monitoring (IEC 61724-1, Edition 1.0, 2017-03), (2017).
- [19] E.F. Fernández, A.J.G. Loureiro, G.P. Smestad, Multijunction Concentrator Solar Cells: Analysis and Fundamentals, in: P. Pérez-Higueras, E.F. Fernández (Eds.), *High Conc. Photovoltaics Fundam. Eng. Power Plants*, Springer International Publishing, 2015. doi:10.1007/978-3-319-15039-0.
- [20] E.F. Fernández, P. Pérez-Higueras, A.J. Garcia Loureiro, P.G. Vidal, Outdoor evaluation of concentrator photovoltaic systems modules from different manufacturers: first results and steps, *Prog. Photovoltaics Res. Appl.* 21 (2012) 693–701. doi:10.1002/pip.1262.
- [21] E.F. Fernández, A. Soria-Moya, F. Almonacid, J. Aguilera, Comparative assessment of the spectral impact on the energy yield of high concentrator and conventional photovoltaic technology, *Sol. Energy Mater. Sol. Cells*. 147 (2016) 185–197. doi:http://dx.doi.org/10.1016/j.solmat.2015.12.003.
- [22] Deutsche Gesellschaft Für Sonnenenergie (Dgs), *Planning and Installing Photovoltaic Systems: A Guide for Installers, Architects and Engineers*, Routledge, 2007.
- [23] N. Martin, J.M. Ruiz, A New Method for the Spectral Characterisation of PV modules, *Prog. Photovoltaics Res. Appl.* 7 (1999) 299–310.
- [24] G. Nofuentes, B. García-domingo, J. V Muñoz, F. Chenlo, Analysis of the dependence of the spectral factor of some PV technologies on the solar spectrum distribution, *Appl. Energy*. 113 (2014) 302–309. doi:10.1016/j.apenergy.2013.07.044.

- [25] C.A. Gueymard, D.R. Myers, Evaluation of conventional and high-performance routine solar radiation measurements for improved solar resource, climatological trends, and radiative modeling, *Sol. Energy*. 83 (2009) 171–185. doi:10.1016/j.solener.2008.07.015.
- [26] T. Ishii, K. Otani, T. Takashima, Y. Xue, Solar spectral influence on the performance of photovoltaic (PV) modules under fine weather and cloudy weather conditions, *Prog. Photovoltaics Res. Appl.* 15 (2011) n/a–n/a. doi:10.1002/pip.1210.
- [27] A. Luque, S. Hegedus, *Handbook of Photovoltaic Science and Engineering*, John Wiley & Sons, Ltd, Chichester, UK, 2003. doi:10.1002/0470014008.
- [28] M. Torres-Ramírez, G. Nofuentes, J.P. Silva, S. Silvestre, J. V. Muñoz, Study on analytical modelling approaches to the performance of thin film PV modules in sunny inland climates, *Energy*. 73 (2014) 731–740. doi:10.1016/j.energy.2014.06.077.
- [29] G. Nofuentes, C.A. Gueymard, J. Aguilera, M.D. Pérez-Godoy, F. Charte, Is the average photon energy a unique characteristic of the spectral distribution of global irradiance?, *Sol. Energy*. 149 (2017) 32–43. doi:10.1016/j.solener.2017.03.086.
- [30] D. Dirnberger, G. Blackburn, B. Müller, C. Reise, On the impact of solar spectral irradiance on the yield of different PV technologies, *Sol. Energy Mater. Sol. Cells*. 132 (2014) 431–442. doi:10.1016/j.solmat.2014.09.034.
- [31] J. Zorrilla-Casanova, M. Piliouguine, Analysis of dust losses in photovoltaic modules, in: *World Renew. Energy Congr.*, Linköping (Sweden), 2011: pp. 2985–2992. doi:10.3384/ecp110572985.
- [32] E.F. Fernández, J.P. Ferrer-Rodríguez, F. Almonacid, P. Pérez-Higueras, Current-voltage dynamics of multi-junction CPV modules under different irradiance levels, *Sol. Energy*. 155 (2017) 39–50. doi:10.1016/j.solener.2017.06.012.
- [33] S. Senthilarasu, E.F. Fernández, F. Almonacid, T.K. Mallick, Effects of spectral coupling on perovskite solar cells under diverse climatic conditions, *Sol. Energy Mater. Sol. Cells*. 133 (2015) 92–98. doi:10.1016/j.solmat.2014.10.037.